Journal of Geophysical Research: Oceans

RESEARCH ARTICLE
10.1029/2018JC013895

Key Points:
- Variability of the ISOW transport at the CGFZ is correlated with the variability of the barotropic transport associated with the NAC front
- Variability of ISOW transport at the CGFZ may be induced by large-scale zonal wind in the Western European Basin east of the CGFZ
- The westward ISOW transport through the CGFZ is anticorrelated with the southward transport along the eastern flank of the MAR

Correspondence to:
X. Xu,
xxu3@fsu.edu

Citation:
Xu, X., Bower, A., Furey, H., & Chassignet, E. P. (2018). Variability of the Iceland-Scotland overflow water transport through the Charlie-Gibbs fracture zone: Results from an eddying simulation and observations. *Journal of Geophysical Research: Oceans*, *123*. https://doi.org/10.1029/2018JC013895

Received 8 FEB 2018
Accepted 31 JUL 2018
Accepted article online 8 AUG 2018

Variability of the Iceland-Scotland Overflow Water Transport Through the Charlie-Gibbs Fracture Zone: Results From an Eddying Simulation and Observations

Xiaobiao Xu[1], Amy Bower[2], Heather Furey[2], and Eric P. Chassignet[1]

[1]Center for Ocean-Atmospheric Prediction Studies, Florida State University, Tallahassee, FL, USA, [2]Woods Hole Oceanographic Institution, Woods Hole, MA, USA

Abstract Observations show that the westward transport of the Iceland-Scotland overflow water (ISOW) through the Charlie-Gibbs Fracture Zone (CGFZ) is highly variable. This study examines (a) where this variability comes from and (b) how it is related to the variability of ISOW transport at upstream locations in the Iceland Basin and other ISOW flow pathways. The analyses are based on a 35-year 1/12° eddying Atlantic simulation that represents well the main features of the observed ISOW in the area of interest, in particular, the transport variability through the CGFZ. The results show that (a) the variability of the ISOW transport is closely correlated with that of the barotropic transports in the CGFZ associated with the meridional displacement of the North Atlantic Current front and is possibly induced by fluctuations of large-scale zonal wind stress in the Western European Basin east of the CGFZ; (b) the variability of the ISOW transport is increased by a factor of 3 from the northern part of the Iceland Basin to the CGFZ region and transport time series at these two locations are not correlated, further suggesting that the variability at the CGFZ does not come from the upstream source; and (c) the variability of the ISOW transport at the CGFZ is strongly anticorrelated to that of the southward ISOW transport along the eastern flank of the Mid-Atlantic Ridge, suggesting an out-of-phase covarying transport between these two ISOW pathways.

Plain Language Summary The Iceland-Scotland overflow water (ISOW) is a dense water mass that originates in the Nordic Seas and spills into the North Atlantic Ocean through gaps between the Iceland and Scotland. It flows southward in the deep Iceland Basin in multiple branches, one of which turns westward through the Charlie-Gibbs Fracture Zone (CGFZ) near 35°W, 53°N. Observations at this critical location revealed that the flow is highly variable, sometimes even reversed to flow eastward. This study uses a numerical model to investigate the source of the variability and the relationship of the variability found at this location to other places. The model reproduces most of the observed ISOW variability. The results suggest that the ISOW variability in the deep ocean is linked to a north-south shift of the current in the upper ocean and is possibly induced by fluctuations of large-scale wind in east-west direction. Furthermore, the ISOW at the CGFZ is much more variable than its upstream source in the northern and central Iceland Basin, and the westward flow through the CGFZ varies together, in an opposite phase, with a southward flowing branch along the eastern flank of the Mid-Atlantic Ridge.

1. Introduction

Flow over the Greenland-Iceland-Scotland Ridge provides two sources of Nordic Seas overflow water into the northern North Atlantic. The western source flows through the Denmark Strait and it forms the Denmark Strait overflow water (DSOW) that is observed to flow down the slope in the western Irminger Sea (e.g., Bacon & Saunders, 2010; Dickson et al., 2008). The eastern source consists of (a) flows over the Iceland-Faroe Ridge (e.g., Beaird et al., 2013), (b) flows through the Faroe-Shetland Channel and then the Faroe Bank Channel (e.g., Hansen & Østerhus, 2007), and (c) a small spill over the Wyville-Thomson Ridge into the Rockall trough (e.g., Sherwin & Turrell, 2005). The flows over the Iceland-Faroe Ridge and through the Faroe Bank Channel combine to form the Iceland-Scotland overflow water (ISOW), which continues southwestward along the northwestern slope of the Iceland Basin. Further south, most of the ISOW is thought to flow westward through the Charlie-Gibbs Fracture Zone (CGFZ). The distributions of salinity and other tracers in the Irminger Sea suggest that, after flowing through the CGFZ, the ISOW consequently turns northward into the Irminger Sea and joins the DSOW there (e.g., Dickson & Brown, 1994; Hansen & Østerhus, 2000; Livingston et al., 1985; Saunders, 2001).

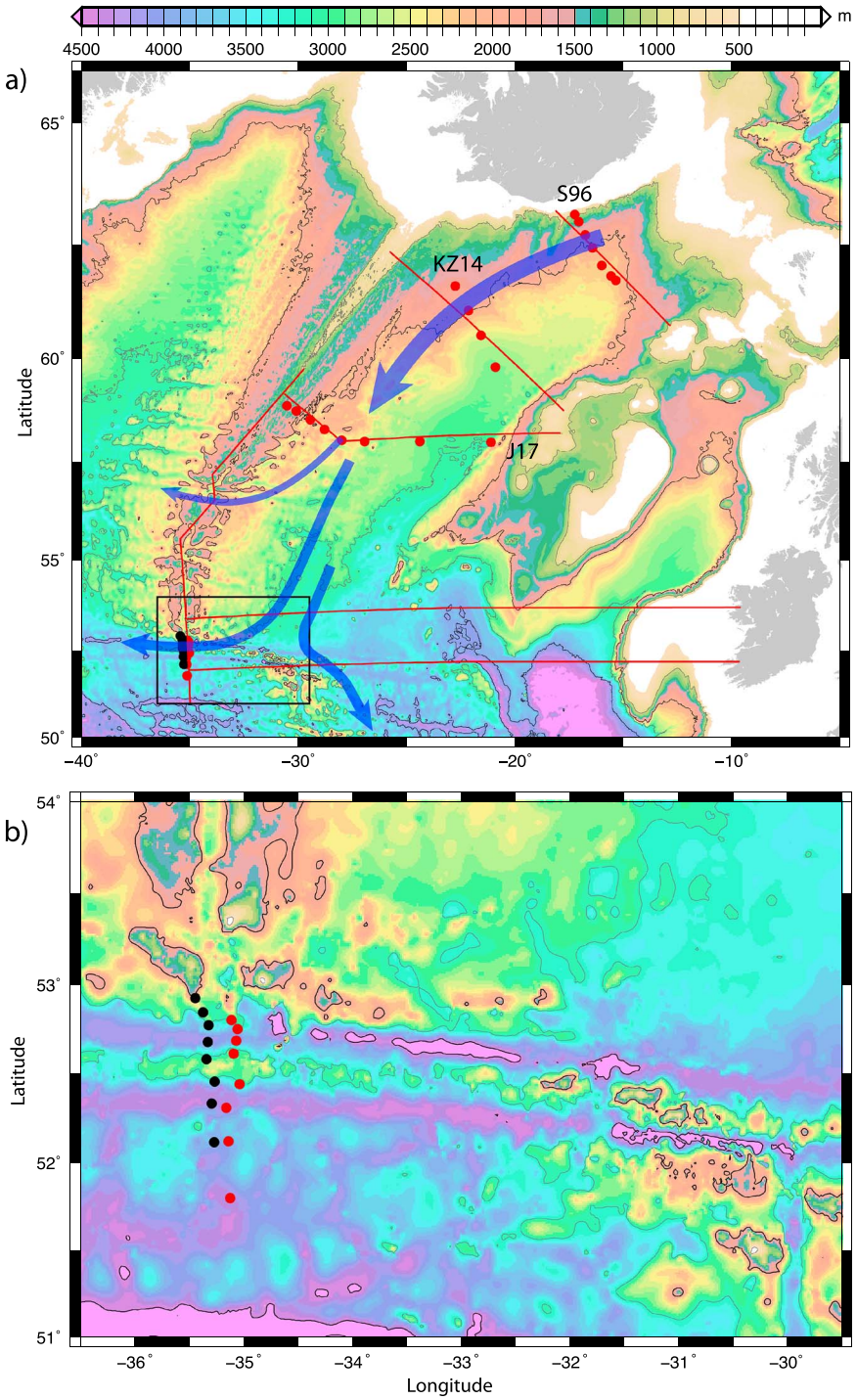

Figure 1. Bathymetry of (a) the Iceland Basin in the northern North Atlantic. (b) The Charlie-Gibbs fracture zone (CGFZ) as denoted by the black box in (a). The 1,000- and 3,000-m isobaths are contoured in gray and 2,000 and 4,000 m in black. The blue arrows indicate the southward flow pathways of the ISOW. The red dots in the Iceland Basin indicate the location of three mooring arrays reported in Saunders (1996), Kanzow and Zenk (2014), and Johns et al. (2017), also labeled S96, KZ13, and J17, respectively. The red lines denote the model sections across which the transports are examined. The red and black dots in the CGFZ mark the two mooring arrays of Saunders (1994) and Bower and Furey (2017), respectively.

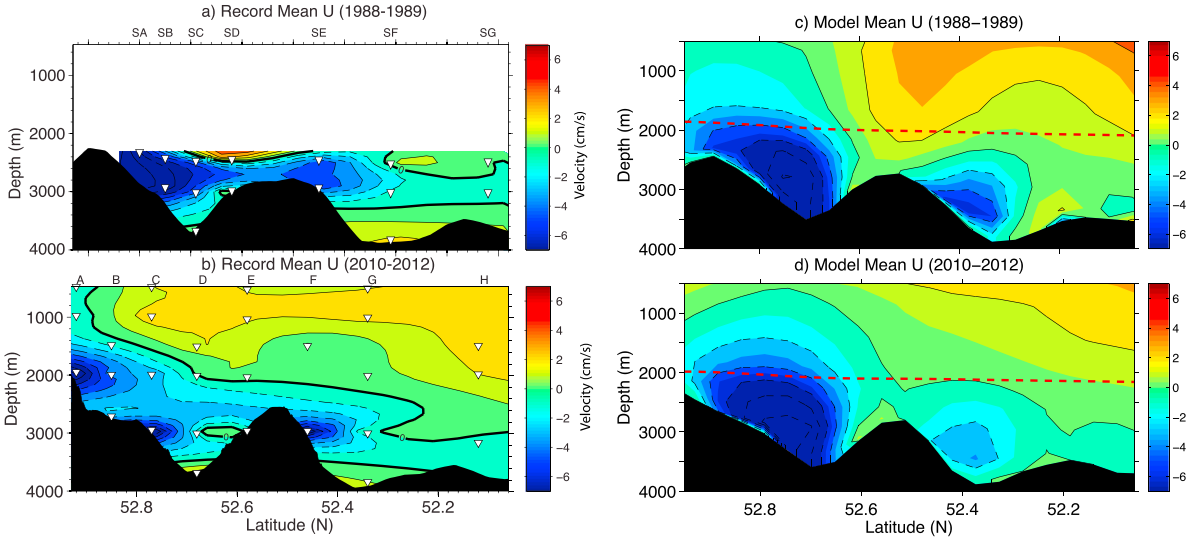

Figure 2. (a and b) Vertical-meridional distribution of the time mean zonal velocity across the Charlie-Gibbs fracture zone (CGFZ) based on observations in 1988–1989 and 2010–2012. (c and d) Results based on numerical simulation along the closest model grid line for the same observation periods. The dashed red line denotes density (σ_2) surface of 36.93 kg/m^3, which is used to define ISOW.

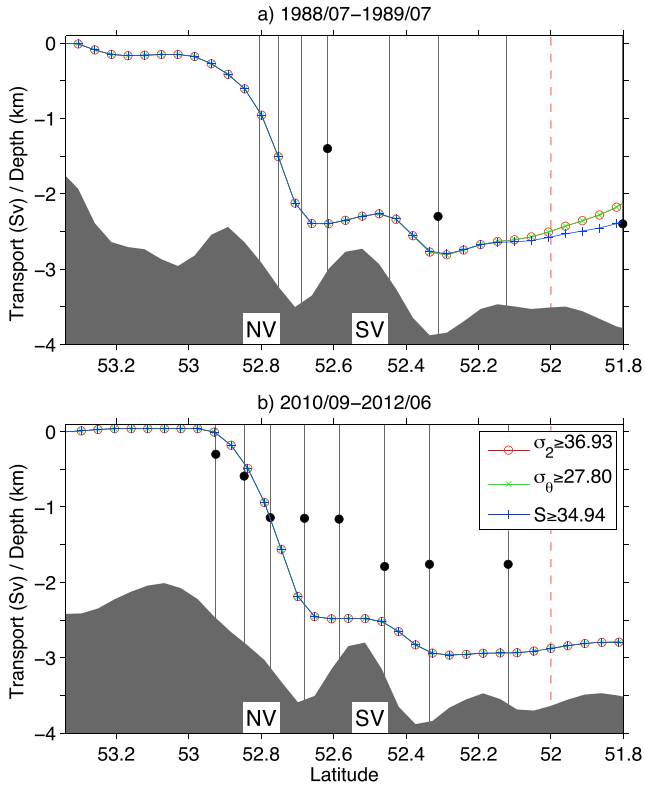

Figure 3. Southward accumulation of the modeled mean ISOW transports in (a) 1988–1989 and (b) 2010–2012 in the CGFZ with different definitions for the ISOW. The black dots are observation-based mean transports from Saunders (1994, Table 5) and Bower and Furey (2017, Table 2), respectively. The vertical lines denote the mooring locations; NV and SV are northern and southern valleys of the CGFZ.

The DSOW and ISOW, together with the Labrador Sea Water (LSW) that is formed within the subpolar North Atlantic, constitute the North Atlantic Deep Water (NADW) that flows southward as the lower limb of the Atlantic meridional overturning circulation (AMOC). Knowledge of the circulation pathway and transport for each of these components, including the temporal variability, is fundamental in understanding the AMOC. Of particular interest in this study is the ISOW, characterized by a relatively high salinity ($S > 34.94$) in the water column below density surface of (σ_θ) 27.80 kg/m^3. In the Iceland Basin, the southward flow of the ISOW has been observed with long-term current meter moorings at three key locations (see Figure 1a): southeast of Iceland near 16°W (3.2 Sv; Saunders, 1996), south of Iceland near 22°W (3.8 Sv; Kanzow & Zenk, 2014), and in the central Iceland Basin across 58°N (5.6 Sv; Johns et al., 2017). Further south, ISOW has been observed to flow westward through the CGFZ (Figure 1b) with its transport measured twice by two mooring arrays: 2.4 Sv in 1988–1989 by Saunders (1994) and 1.7 Sv in 2010–2012 by Bower and Furey (2017).

The mean ISOW transport measured through the CGFZ is smaller than the upstream values obtained in the northern and central Iceland Basin. This implies that the ISOW must exit the Iceland Basin via pathways other than the CGFZ. Several authors (Fleischmann et al., 2001; Hansen & Østerhus, 2000; Xu et al., 2010; and Zou et al., 2017) have proposed that the ISOW may exit the Iceland basin via a westward flow through gaps in the Reykjanes Ridge north of the CGFZ and/or via a southward flow along the eastern flank of the Mid-Atlantic Ridge (MAR) south of the CGFZ.

One of the most striking features of the observed ISOW transport in the CGFZ is that it exhibits very large temporal variability, with frequent reversals (Bower & Furey, 2017; Saunders, 1994). Saunders (1994) surmised that the large-amplitude overflow reversals might be connected to latitudinal migrations of the North Atlantic Current (NAC) over the CGFZ, an

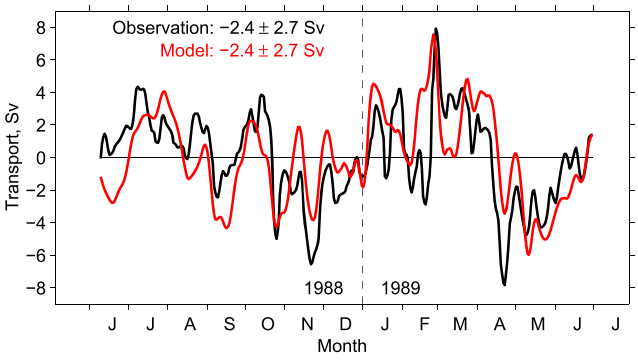

Figure 4. Variability of the observed and modeled ISOW transports through the CGFZ in 1988–1989. The observations (black line) are from Saunders (1994, Figure 10); the model results (red line) are from an 1/12° Atlantic simulation and are low-passed using a 5-day top-hat filter as in Saunders (1994). The numbers are mean and standard deviation values.

assumption that was supported by the subsequent observations of Belkin and Levitus (1996) and Schott et al. (1999). Using empirical orthogonal function analysis and maps of the satellite-derived absolute dynamic topography, Bower and Furey (2017) showed that the ISOW transport events, including complete reversals, are indeed related to the northward meandering of the NAC. In this paper, we investigate further the CGFZ variability by using a high-resolution numerical model that has been shown to be in good agreement with the observations. Specifically, we address the following questions:

1. Where does the ISOW transport variability come from? Is the ISOW transport variability solely connected to the variability of NAC transport in the CGFZ? Are there other factors contributing to the variability?
2. Since the CGFZ is only one of the ISOW pathways out of the Iceland basin, how does the CGFZ variability relate to that of the other pathways and to the transport further upstream in the northern Iceland Basin?

We find that (i) variability of ISOW transport through the CGFZ is closely correlated with the barotropic transport variability in the CGFZ and is likely forced by the variation of zonal wind stress in the Western European Basin to the east of the CGFZ; (ii) the variability of the ISOW transport increases by a factor of 3 between the northern part of the Iceland Basin and the CGFZ, and they are not correlated, confirming that the variability at the CGFZ does not come from the upstream source; and (iii) the variability at the CGFZ is strongly anticorrelated with that of the southward ISOW transport along the eastern flank of the Mid-Atlantic Ridge, suggesting an out-of-phase covarying transport between these two ISOW pathways.

The paper is organized as follows: section 2 briefly summarizes the key observations in the CGFZ and the model simulation. In section 3, we show that the modeled ISOW structure and variability in the CGFZ are representative of the observations. We then use the model results in section 4 to examine the source of the ISOW transport variability, in particular, its relationship with the NAC transport as well as with the large-scale wind stress in the northern North Atlantic. In section 5, we examine the large-scale context of the CGFZ transports, for example, its connection to the upstream source in the Iceland Basin and to the other ISOW pathway to the south along eastern flank of the MAR. Finally, the results are summarized and discussed in section 6.

2. Observations and Numerical Simulation

2.1. Observations

The main observations used in this study are ISOW transports through the CGFZ obtained from two mooring arrays: Saunders (1994) from June 1988 to July 1989 and, more recently, Bower and Furey (2017) from August 2010 to June 2012. The 2010–2012 array is deployed nominally along 35.33°W, spanning a latitudinal range between 52.925°N and 52.118°N (Figure 1b). Five of the eight moorings are located in the northern valley, where strong current of ISOW is observed, and three were in the southern valley and plain. There are four tall moorings with the instruments extending from the seafloor to 500 m and four shorter moorings with the instruments extending to 1,500 m. In total, there are 28 current meters measuring current speed and direction and 36 SBE-37 microcats measuring temperature and conductivity. Compared to the 1988–1989 array, the 2010–2012 array is more substantial in that (a) the current velocity is measured with more instruments, thus providing a better vertical coverage for a longer period of time, and (b) both temperature and salinity are continuously sampled so that the ISOW interface is determined with confidence.

The basic structure of the velocity distributions obtained from the 2010–2012 array is consistent with Saunders (1994) (see Figures 2a and 2b and detailed discussions in Bower and Furey (2017)). The most substantial difference is that the 22-month mean westward transport is 1.7 ± 0.5 Sv (Bower & Furey, 2017), 30% lower compared to the 13-month mean of 2.4 ± 1.2 Sv in Saunders (1994). The difference between these two transport estimates is mostly due to the difference in measured thickness (of the ISOW layer). Uncertainties are greater in Saunders (1994) since his estimate of the thickness of the ISOW layer was based on one

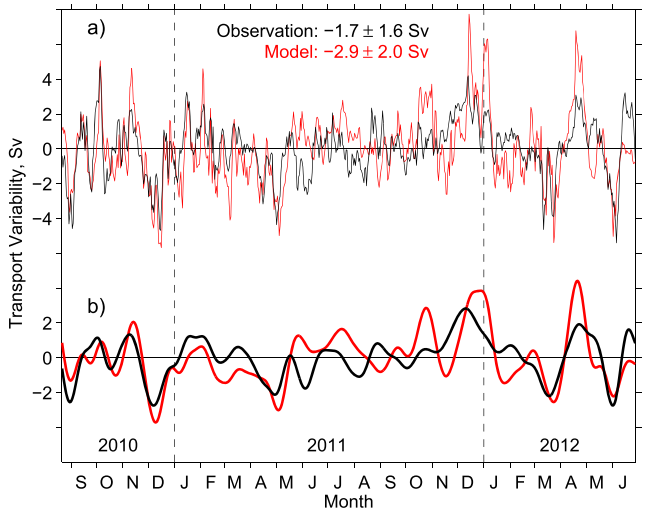

Figure 5. Variability of ISOW transports through the CGFZ in 2010–2012, based on observations (black lines) and an 1/12° numerical simulation (red lines). (a) Original daily mean time series. (b) Low-passed by a third-order, 30-day Butterworth filter as in Bower and Furey (2017). The numbers are mean and standard deviation values based on unfiltered daily mean transports.

hydrographic survey versus continuously in Bower and Furey (2017). However, it is important to note that this 30% difference in mean ISOW transport is not statistically significant given the short time series and the very large transport variability.

2.2. Numerical Simulation

The numerical configuration used for this study was described by Xu et al. (2013). The 1/12° eddying Atlantic simulation is based on the HYbrid Coordinate Ocean Model (HYCOM; Bleck, 2002; Chassignet et al., 2003; Halliwell, 2004). The atmospheric forcing is from the European Center for Medium-Range Weather Forecasts (ECMWF) reanalysis ERA40 (Uppala et al., 2005) for 1978–2001 and the Fleet Numerical Meteorology and Oceanography Center (FNMOC) Navy Operational Global Atmospheric Prediction System (NOGAPS; Rosmond et al., 2002) for 2002–2012. Xu et al. (2013) show that the simulation is overall in good agreement with observations. In particular, the model represents well the observed western boundary transports of LSW, ISOW, and DSOW near 53°N and 43°N, and the structure of the transbasin AMOC determined from hydrographic data along the WOCE-AR19 line near 48°N. The model also represents well the observed sea surface height (SSH) changes in central Labrador Sea since early 1990s, from which Häkkinen and Rhines (2004) inferred a significant decline in the subpolar gyre transport. The modeled subpolar gyre and AMOC undergo decadal variability as a lagged response to the fluctuations of the North Atlantic Oscillation (NAO), generally consistent with other model results (e.g., Biastoch et al. 2008).

3. Observed and Modeled ISOW in the CGFZ

In this section, we compare the model results with the observations in the CGFZ to show that the numerical simulation represents well the key features of the observed ISOW at this location. Figure 2 displays the time mean zonal velocity across the CGFZ for both 1988–1989 and 2010–2012 periods in the observations (Figures 2a and 2b) and in the model (Figures 2c and 2d). Both the observations and model results show a strong westward flow of ISOW in the northern valley and a weaker westward flow in the southern valley. The velocity contrast between the two valleys is larger in the model.

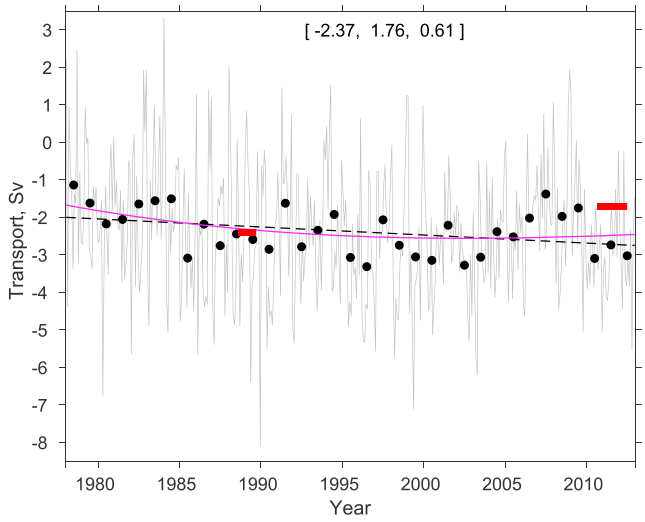

Figure 6. Modeled ISOW transports through the CGFZ from 1978 to 2012. Gray line and black dots denote monthly and annual means, respectively. Dashed black and solid pink lines denote the long-term trend determined by a linear fit (−0.215 Sv per decade) and by using the ensemble empirical mode decomposition (EEMD; Wu & Huang, 2009). The two short red lines denote the mean transports based on observations of Saunders (1994) and of Bower and Furey (2017). The three bracketed numbers are 35-year mean and two standard deviation values based on monthly and annual mean transports.

The mean volume transport of the modeled ISOW is shown in Figure 3. The ISOW, due to mixing with the (warm) salty modified North Atlantic Water (MNAW; Hansen & Østerhus, 2000) during its initial descent near the Iceland-Faroe Ridge, has a distinct signature of high salinity compared to the relative fresh LSW above and Lower Deep Water below. Several definitions, $\sigma_2 > 36.93$ kg/m^3, $\sigma_\theta > 27.80$ kg/m^3, and salinity $S > 34.94$ psu, have been used to identify the ISOW transports (e.g., Bower & Furey, 2017; Saunders, 1994) and they are examined in Figure 3. The ISOW transport in the CGFZ is defined as the flow within latitude range from 53.3°N to 52°N to ensure that all ISOW is accounted for. The modeled 13-month mean westward transport of the ISOW in 1988–1989 (2.4 Sv) is close to observations. However, the modeled 22-month mean ISOW transport in 2010–2012 is higher (2.9 Sv), compared to 1.7 Sv in observations. In both the observations and the model, most of the ISOW transport comes from the northern valley (1.1 versus 0.6 Sv in the observations and 2.5 versus 0.4 Sv in the model). Also, the ISOW transports in the two valleys are not correlated in both observations and model.

Figure 4 compares the observed and modeled ISOW transport variability during the 1988–1989 period as in Saunders (1994). Both time series are

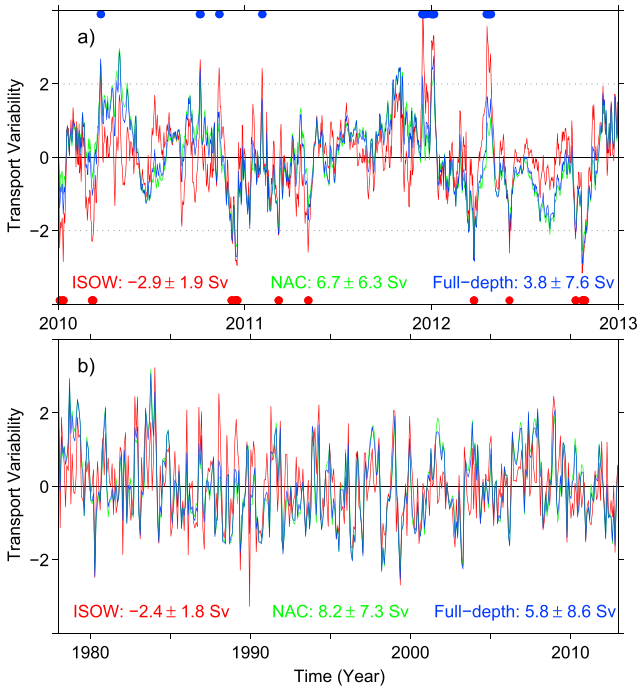

Figure 7. Variability of the modeled ISOW (red), NAC (green), and full-depth (blue) transports through the CGFZ. (a) Daily means from 1 January 2010 to 31 December 2012. (b) Monthly means from January 1978 to December 2012. The mean ± standard deviation values for each transports are listed; the variability is normalized by the standard deviation. The blue/red dots in (a) denotes the days when the model westward ISOW transports are extremely weak/strong (outside of 2 times of the standard deviation).

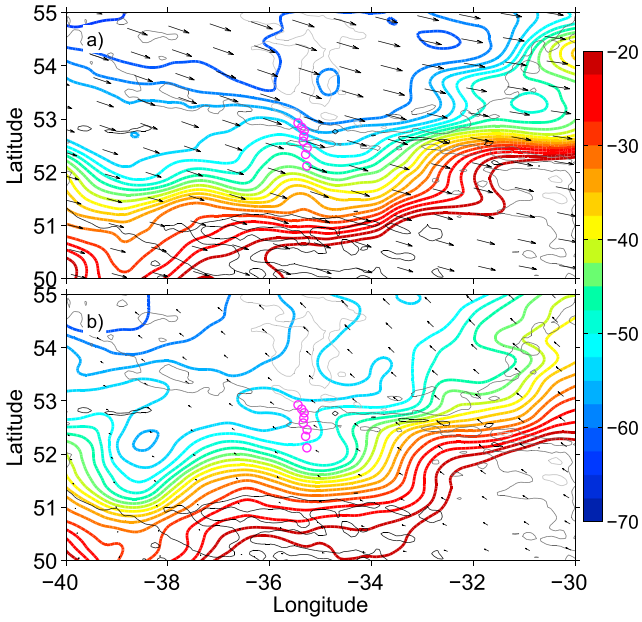

Figure 8. Composites of the modeled sea surface height (SSH; in cm) in the CGFZ region for (a) 33 days of weak ISOW transport and (b) 34 days of strong ISOW transports in 2010–2012 (denoted in blue/red dots in Figure 7a). The black vectors denote the corresponding composite wind stress; magenta circles denote location of the mooring array in the CGFZ.

low-passed using a 5-day top-hat filter. The two transport time series are very similar, with a high correlation coefficient *C* of 0.63 (significant above 99.9% level). Figure 5 compares the variability of observed and modeled transports for the 22-month period from 2010 to 2012 (daily mean in Figure 5a and low-passed in Figure 5b). The magnitude of the modeled transport variability is slightly higher than observations (2.0 versus 1.6 Sv in the standard deviation for daily mean transports), but the two transport time series are very similar, with a high correlation coefficient *C* of 0.64 for the unfiltered time series and 0.65 for the low-passed time series.

Can the observed mean transport difference between 1988–1989 and 2010–2012 be an indicator of long-term variability of the ISOW transport? To examine this, Figure 6 displays the modeled monthly and annual mean transports for the 35-year period from 1978 to 2012. The modeled ISOW transport does exhibit long-term variability. A linear fit of both the monthly- and annual-mean time series gives an increasing transport trend of 0.215 Sv per decade (dashed black line in Figure 6; negative transports meaning westward). This trend, while sufficient to explain the modeled 0.5-Sv difference between the two time periods, is not very robust. Using the Theil-Sen robust estimator, we find that the trend determined from monthly mean time series is significant at 95% level, but that the trend determined from the annual mean time series is not. A more careful analysis of the time series using the ensemble empirical mode decomposition of Wu and Huang (2009) shows a nonlinear long-term variability (pink line in Figure 6), with the westward transport increasing by about 0.9 Sv for the first 25 years and decreasing by about 0.1 Sv for the last 10 years. This long-term variability explains only one third of the modeled 0.5-Sv difference between the two time periods. On interannual time scales, the modeled ISOW transport exhibits significant variability; that is, the 35 annual mean transports have a standard deviation of 0.6 Sv. Thus, the 0.7-Sv observed difference between 1988–1989 and 2010–2012 could simply be explained by interannual variability rather than a long-term trend.

Finally, the standard deviation of the modeled monthly mean transports is about 1.8 Sv for the 35-year time series. It is 2.0 Sv for 1988–1989 and 1.2 Sv for 2010–2012 (compared to 2.1 and 1.0 Sv in observations). Thus, a 2-year-long measurement is still relatively short and may not necessarily be representative of the long-term mean and variability statistics.

4. Source of the ISOW Transport Variability in the CGFZ

The strong intraseasonal variability of ISOW transports in the CGFZ was first observed in Saunders (1994). The author speculated that the comparatively large-amplitude overflow reversals might be connected to latitudinal migrations of the NAC over the CGFZ, a speculation that was supported in the subsequent observations in Belkin and Levitus (1996) and Schott et al. (1999). Using empirical orthogonal function analysis and maps of the satellite-derived absolute dynamic topography, Bower and Furey (2017) show that the weak ISOW transport events, including complete reversals, are indeed related to the northward meandering of the NAC. The good agreement between the observed and the modeled ISOW transport variability allows us to use the model results to investigate this relationship in more detail and put it in a broader perspective.

Figure 7a compares the variability of the modeled daily mean transports of the ISOW, the NAC transport above the ISOW, and the full-water column

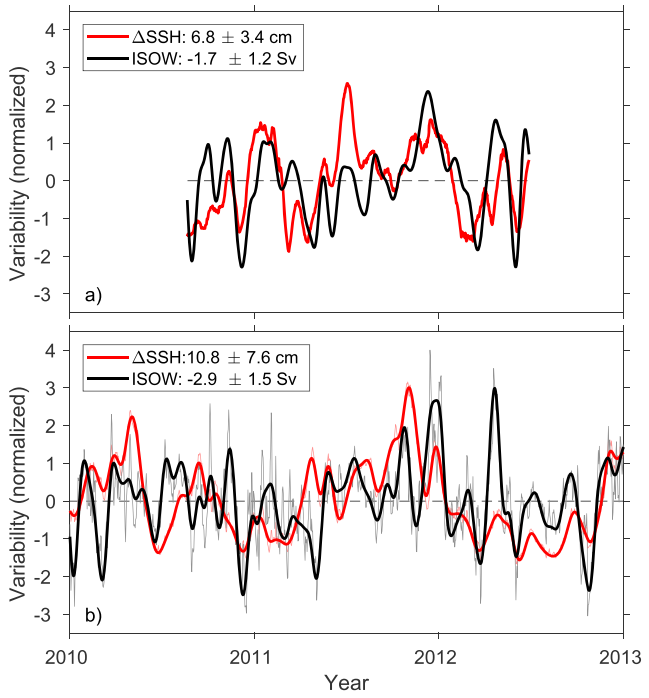

Figure 9. (a) Variability of the observed ISOW transport (low-passed by third-order, Butterworth filter) and the sea surface height (SSH) difference across the CGFZ between 52.125 and 53.125°N along 35.25°W, both normalized by the standard deviation value. (b) Variability of the modeled ISOW transports and SSH difference across the CGFZ between 52.125 and 53.125°N along 35.25°W (thin lines denote daily mean time series and thick lines denote low-passed results).

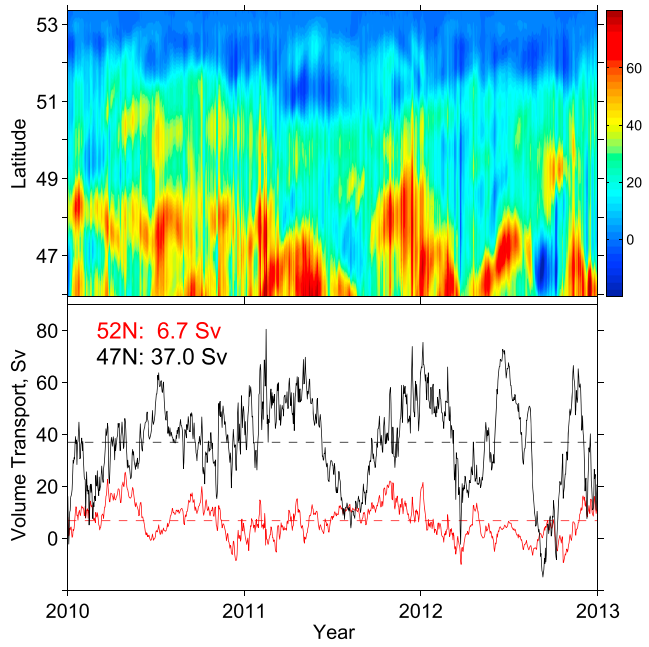

Figure 10. (a) Southward accumulation of the modeled eastward NAC transports along 35°W from 53.3°N to 46°N in 2010–2012. (b) Time series of the modeled NAC transports integrated (from 53.3°N) to 52°N (red line) and to 47°N (black line).

barotropic transport in 2010–2012. All three time series are normalized with their standard deviation values, as the variability of the NAC is much higher than the ISOW. The ISOW and NAC transports are highly correlated ($C = 0.62$, significant above 99.9% level), and the correlation is even higher between ISOW and the full water column barotropic transports ($C = 0.76$). The variability of NAC and barotropic transports is essentially the same ($C = 0.98$). The high correlation applies on longer time scales as well: the correlation coefficient is 0.68 between the ISOW and the NAC, 0.78 between the ISOW and the barotropic transports, and 0.98 between the NAC and the barotropic transports for the modeled 35-year monthly mean transport time series from 1978 to 2012 (Figure 7b).

The high correlations between the ISOW and NAC transports on one hand and between the NAC and the barotropic transport on the other suggest that, although the mean flow structure in the CGFZ is mostly baroclinic (i.e., eastward flow in the upper layer and westward flow in the deeper layer; Figure 2), the ISOW variability is, to a large degree, barotropic and is connected to the meridional displacement or meandering of the NAC front. To further examine the relationship between the ISOW transport and the NAC frontal position, we select all the days in 2010–2012 when the modeled westward ISOW transport is weaker (stronger) than the 3-year mean by 2 times of the standard deviation, as marked in blue (red) dots in Figure 7a. The composite model SSH for these extremely weak and strong ISOW transport events (33 and 34 days, respectively) are shown in Figures 8a and 8b. The model results are consistent with Bower and Furey (2017); that is, the weak westward ISOW transport is associated with a stronger NAC front (indicated by the SSH gradient) in the CGFZ, whereas the strong ISOW transport is associated with a weaker NAC front.

One can also demonstrate the latter by directly comparing the ISOW transport and the SSH gradient time series in the observations and in the model. Figure 9a shows the ISOW transport variability from Bower and Furey (2017) and the absolute dynamic topography difference along 35°W (between 53.125°N and 52.125°N) based on 1/4° AVISO. The low-pass filtered ISOW transport variability is used here to be comparable to the spatially and temporally filtered AVISO products. The correlation ($C = 0.50$) is significant on 99% level, suggesting that part of the observed ISOW transport variability can be inferred from satellite-based SSH data. The correlation is lower between the modeled ISOW transport and SSH difference for the same latitudinal range (with $C = 0.40$; Figure 9b and later in Figure 11c) but is significant on 99% level.

It is important to point out that the NAC transport discussed above is only a portion of the total NAC transport and consists of the eastward flow above the ISOW between 53°N and 52°N with a modeled mean transport of 6.7 Sv (Figure 7). Integrating farther to the south along 35°W leads to a higher mean NAC transport (Figure 10a). At 47°N, the modeled 2010–2012 mean eastward NAC transport reaches ~37 Sv. This transport includes the contributions from the subpolar gyre, the upper limb of the AMOC, and the subtropical gyre (see discussions in Bower & von Appen, 2008; Daniault et al., 2016; Roessler et al., 2015). Thus, the eastward flow across 35°W within the CGFZ range is only a small part of the total NAC transport. Furthermore, the variability of the NAC transport within the CGFZ is not correlated with that of the total NAC transport (Figure 10b), consistent with the observations in Roessler et al. (2015). In other words,

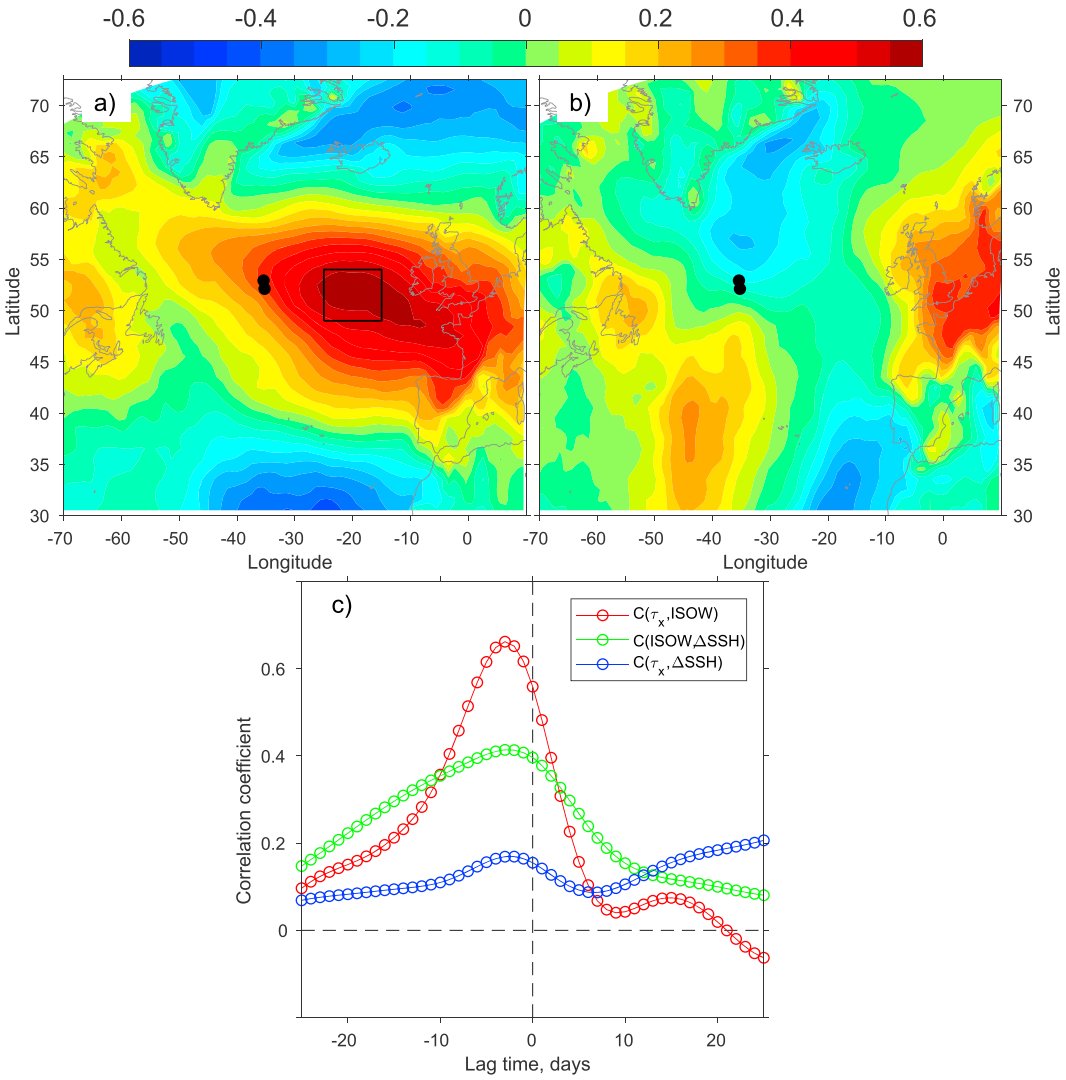

Figure 11. (a and b) Distribution of cross-correlation coefficient at zero lag between the modeled ISOW transport through the CGFZ and (a) zonal wind stress and (b) meridional wind stress in the northern North Atlantic; two black dots mark the location of CGFZ moorings. (c) Lagged cross-correlation coefficients between the zonal wind stress in the western European Basin east of the CGFZ (black box in (a)), the ISOW transport through the CGFZ, and the SSH difference across the CGFZ from 52.125 to 53.125°N. The results show that the zonal wind stress is strongly correlated with the ISOW transport; the ISOW transport is also significantly correlated with the SSH difference. The wind stress, however, is not correlated with the SSH difference.

the ISOW transport variability is linked to the meandering and the eddying activities of the NAC front, not the variability of total NAC transport.

The question then arises as to whether the ISOW transport variability in the CGFZ and the associated meandering of the NAC are purely internal ocean dynamics that are largely stochastic or can be induced externally by atmospheric forcing. As illustrated in Figure 8, we find that the extremely weak and strong ISOW transports are associated with an eastward and westward wind anomaly, respectively. This led us to further examine the relationship between ISOW transport at the CGFZ and wind patterns. Figures 11a and 11b display the cross-correlation coefficient between the ISOW transport at the CGFZ and the zonal/meridional components of the wind stress over the northern North Atlantic. The ISOW transport is highly correlated with the zonal wind stress in the Western European Basin to the east of the CGFZ, with the wind stress variability leading by ~3 days (red line in Figure 11c). Figure 11c also shows that the ISOW transport is correlated with the SSH difference across the CGFZ that represents the northern edge of the NAC front (green line), but the zonal wind stress is not correlated with the SSH difference (blue line). This result shows an indirect relationship between the NAC front and the wind stress. Although the variability of the ISOW transport is shown to be associated

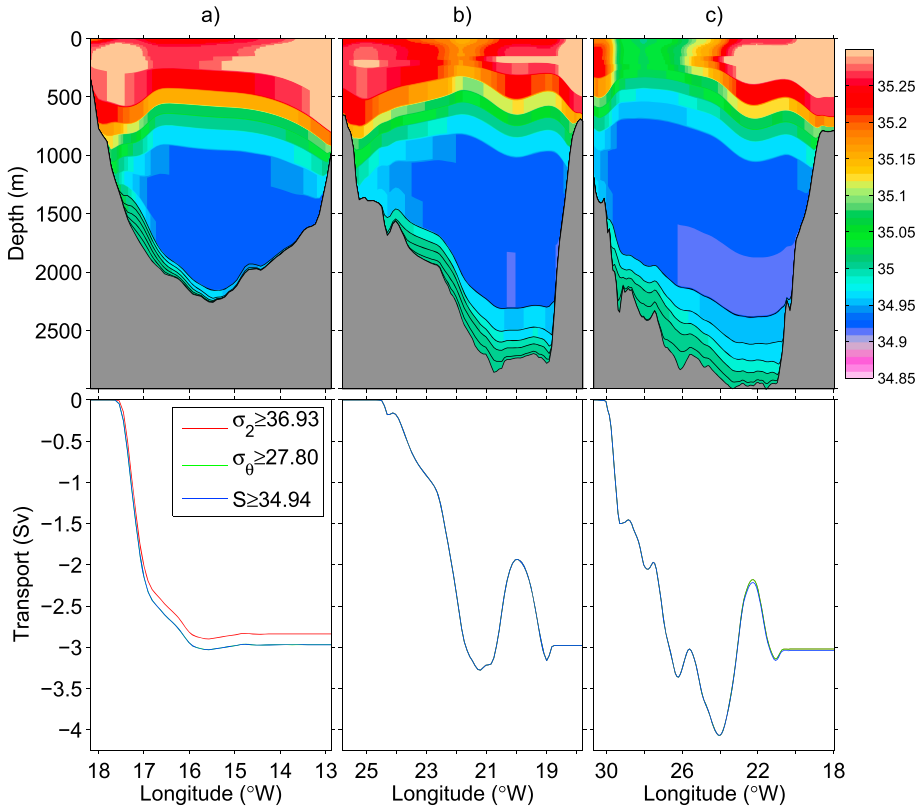

Figure 12. (top) Distribution of the modeled 35-year mean salinity and (bottom) eastward accumulation of the ISOW transports along three sections in the northern and Central Iceland Basin close to (a) Saunders (1996) array at 16°W, (b) Kanzow and Zenk (2014) array at 22°W, and (c) Johns et al. (2017) array at 58°N.

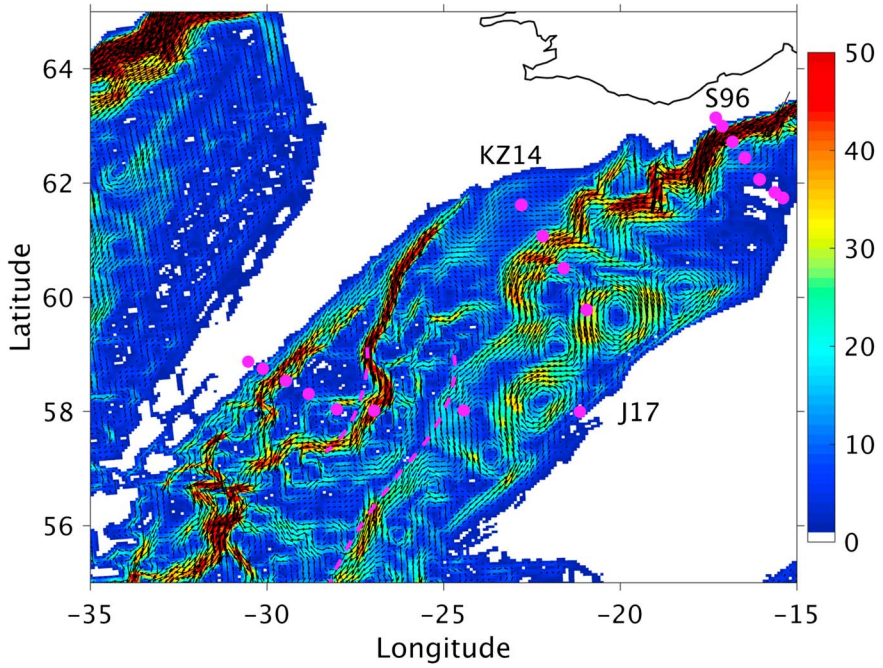

Figure 13. Distribution of the modeled 35-year mean transport per unit width for the ISOW ($\sigma_2 \geq 36.93$ kg/m^3) in the northern and Central Iceland Basin, along with the mooring locations in Saunders (1996), Kanzow and Zenk (2014), and Johns et al. (2017). Dashed magenta lines denote the crest of Björnsson and Gardar drifts, two sedimentary drifts formed by persistent bottom currents.

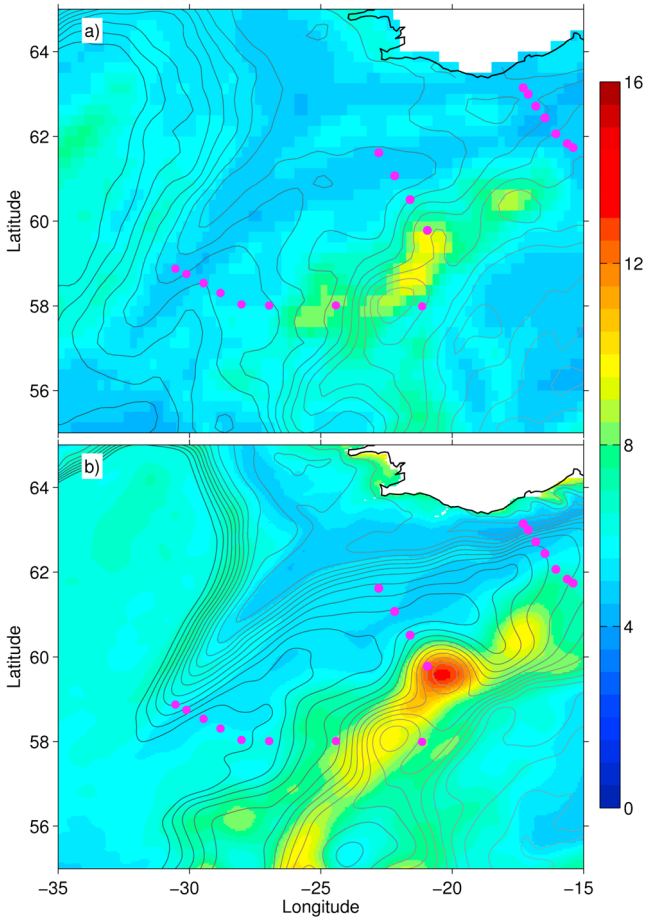

Figure 14. Distribution of the long-term mean (contours) and standard deviation (color shading) of the sea surface height (SSH) in the northern and Central Iceland Basin based on (a) 1/4° AVISO (1993–2012) and (b) the 1/12° Atlantic simulation (1978–2012).

with the meandering of the NAC front in the CGFZ, the latter is not necessarily the causative source for the ISOW transport variability. We also were not able to identify clear propagating signals in the ISOW transport and/or SSH near the CGFZ area. Thus, a process study (i.e., additional numerical experiments with idealized wind stress anomalies) is most likely required to fully determine the cause of ISOW transport variability. This will be the focus of an upcoming work.

5. The Large-Scale Context of the ISOW Transport Through CGFZ

We now discuss the large-scale context of the ISOW transports through CGFZ in terms of time mean and temporal variability. Salinity distribution and transport structure along seven sections (red lines in Figure 1) as well as horizontal maps of the circulation pattern are used to illustrate the time mean circulation structure; the transport variability across the seven sections is used to examine the relationship between the ISOW transport at the CGFZ, the upstream source in the Iceland Basin, and the other ISOW pathways.

Figure 12 shows the modeled (35-year) mean salinity and the ISOW transports for three sections in the northern and central Iceland Basin, close to the three mooring arrays of Saunders (1996), Kanzow and Zenk (2014), and Johns et al. (2017) (Figure 1). The bottom-trapped (relatively) high-salinity ISOW can be seen in all three sections, similar to the observations (see Saunders (1996) for example).

1. Across the Saunders (1996) array southeast of Iceland near 16°W, the modeled mean ISOW transport is 2.8 Sv for $\sigma_2 > 36.93$ (3.0 Sv for $\sigma_0 > 27.80$; Figure 12a). This transport value is only 0.5 Sv higher than the sum of the modeled Iceland-Faroe Ridge and Faroe Bank Channel overflows (which form most of the ISOW), 0.2 and 2.1 Sv, respectively, for $\sigma_2 > 36.93$ (0.3 and 2.2 Sv, respectively, for $\sigma_0 > 27.80$). The modeled ISOW transport near 16°W is similar to the observed 3.2 Sv ($\sigma_0 > 27.80$) of Saunders (1996), which is also not much higher than the sum of the observed transports over the Iceland-Faroe Ridge (0.8 Sv in Beaird et al. (2013)) and the Faroe Bank Channel (2.0 Sv in Hansen and Østerhus (2007)).
2. Downstream across the Kanzow and Zenk (2014) array south of Iceland near 22°W, the modeled mean ISOW transport is 3.0 Sv for $\sigma_2 > 36.93$ (same for $\sigma_0 > 27.80$; Figure 12b). This value is slightly lower than the net southward transport of 3.4 Sv estimated in Kanzow and Zenk (2014). Similarly, the model western boundary current transport (3.2 Sv) is also slightly lower than the 3.8 Sv in Kanzow and Zenk (2014).
3. Farther downstream across the Johns et al. (2017) array near 58°N (Figure 12c), the modeled net ISOW transport is 3.0 Sv and consists of a southwestward transport of 4.0 Sv in three branches west of 24°W and a northward transport of 1 Sv east of 24°W. The salinity in the upper part of the modeled ISOW decreases eastward and the northeastward flow is of fresher water from south that is "entrained" laterally into the ISOW flow. The modeled southward ISOW transport of 4 Sv is significantly lower than the 5.6 Sv as obtained from the observations (Johns et al., 2017). The difference is actually even larger considering that the observed 5.6 Sv is to the west of 26°W and does not include the deeper branch between 24°W and 26°W. The difference, 3.2 versus 5.6 Sv across 58°N west of 26°W, is attributed to a thinner ISOW layer and narrower southward flowing ISOW branches in the model than in observations.

The branching of the modeled ISOW flow in the Iceland basin is illustrated in Figure 13 together with the location of the mooring arrays. The shallowest branch flows closely along the eastern slope of the Reykjanes Ridge, whereas the two deeper branches flow along the crest of Björnsson and Gardar Drifts (dashed lines in Figure 13), two sedimentary drifts formed by the persistent bottom currents. Further east in the deepest portion of the Iceland Basin, one can observe two anticyclonic recirculation cells. These mean circulation patterns

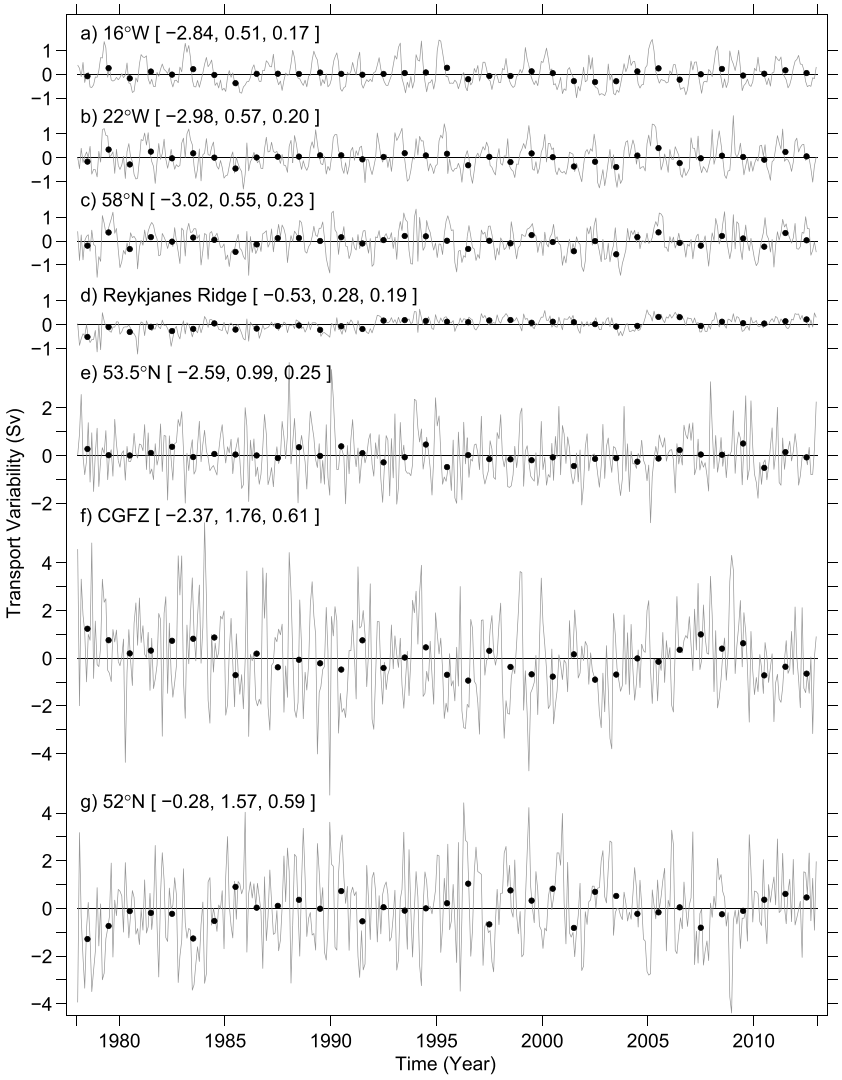

Figure 15. Variability of the modeled ISOW transports at seven sections in the Iceland Basin from 1978 to 2012 (see Figure 1 for the section locations); gray lines and black dots denote monthly means and annual means, respectively. The three bracket numbers are 35-year mean and two standard deviation values base on the monthly and annual mean transports.

are also present in the climatological simulation of Xu et al. (2010), suggesting that they are fairly robust model features. Both the AVISO-based observations and the model exhibit a strong surface signature associated with these recirculations (Figure 14). The modeled SSH variability is stronger and the modeled subpolar gyre also extends further northeastward, before turning westward and flowing around the Reykjanes Ridge as a strong jet following the *f*/*H* (Coriolis parameter/water depth) contours (Treguier et al., 2005). Some of these differences can be attributed to the coarser grid of the AVISO data (Chassignet & Xu, 2017).

The time series of transport variability across the three northern sections are shown in Figures 15a–15c. They exhibit a comparable magnitude of variability, although the standard deviation of the annual mean transports gradually increases downstream from 0.17 to 0.20 and to 0.23 Sv. There is no decreasing or increasing trend over the 35-year integration. The variability of the modeled transports at these three sections is also highly correlated: for monthly mean transports, the correlation coefficient is 0.78 between the 16°W and 22°W sections with a 1-month lag, and 0.52 between 16°W and 58°N with a 4-month lag. The two lag values are 36 and 100 days based on the daily mean transports of 2010–2012, and they are roughly consistent with advection time scales for a distance of ~400 km (between 16°W and 22°W sections) and ~1000 km (between 16°W and 58°N), with an ISOW velocity of 10–15 cm/s. The correlation is even higher for annual mean transports, with a correlation coefficient of 0.91 between 16°W and 22°W (0.92 between 16°W and 58°N).

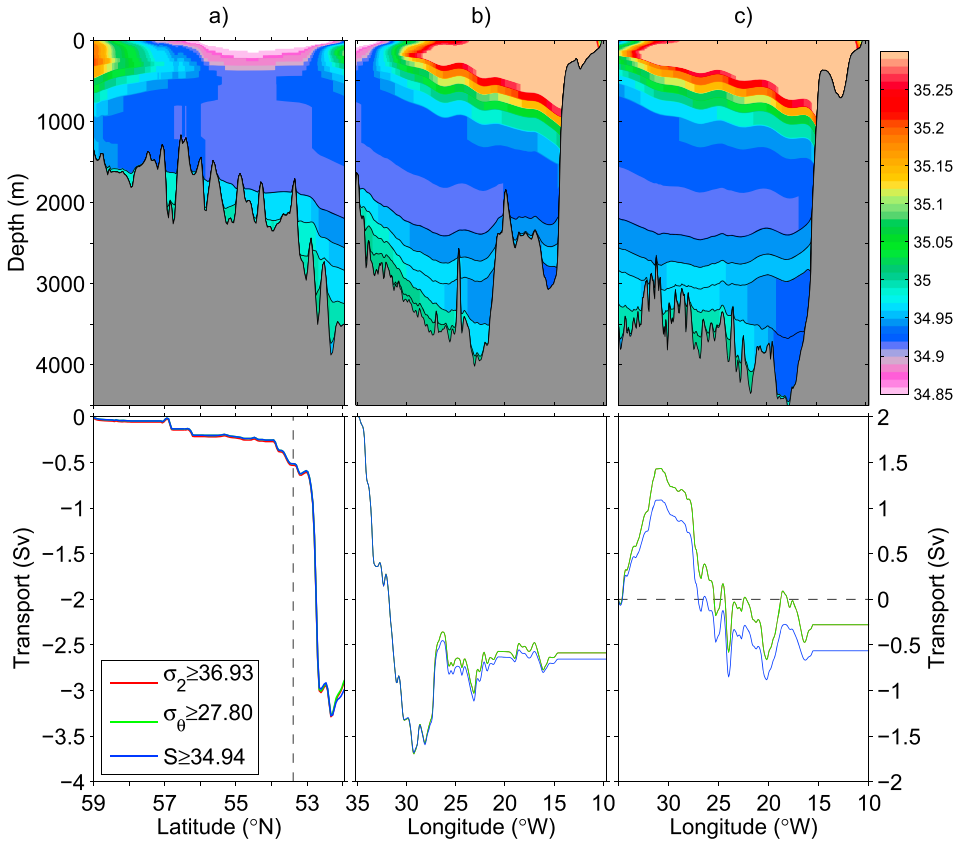

Figure 16. (top) Distribution of the modeled 35-year mean salinity and (bottom) southward/eastward accumulation of the ISOW transports along sections in the southern Iceland Basin and CGFZ regions: (a) the Reykjanes ridge and the CGFZ, (b) 53.3°N, and (c) 52°N (see Figure 1 for the section locations).

We now discuss the four southern sections: (1) along the Reykjanes Ridge, (2) across the CGFZ (which is shown in panel a as an extension of the Reykjanes Ridge), and (3) the two zonal sections near 53.3°N and 52°N. Figure 16 (similar to Figure 12 for the northern sections) displays the distribution of mean salinity and transport.

1. The modeled mean transports across the Reykjanes Ridge (north of CGFZ) and the CGFZ is 0.5 and 2.4 Sv, respectively. The sum of these two transports is similar to the 5-year mean (3.1 Sv) from the climatological simulation of Xu et al. (2010), but in this simulation (with interannual atmospheric forcing), the modeled ISOW transport is stronger through the CGFZ.
2. The modeled net transport across 53.3°N (the northern limit of the CGFZ) is 2.6 Sv, consisting of about 3.6-Sv southward transport west of 30°W and 1-Sv northward flow to the east (which is comparable to 58°N in Figure 12c).
3. The modeled net transport across the 52°N (the southern limit of the CGFZ) is only ~0.2 Sv, consisting of a northeastward flow of 1.5 Sv west of MAR and a southward flow of 1.7 Sv along the eastern flank of the MAR. The northeastward flow west of the MAR is fresher and lighter than the southward flow east of the MAR, and it represents the recirculation in ISOW density range. Rhein et al. (2011) estimated a similar eastward mean transport of 1.2 Sv in ISOW densities from 2 years of PIES (inverted echo sounder with bottom pressure sensor) data obtained west of the MAR (in latitude range 47.6–53°N). Figures 17 and 18 illustrate the large-scale circulation in two layers: in the upper layer ($36.93 < \sigma_2 < 37.00$), the relatively fresh recirculating water from the west basin flows eastward to northeastward through the southern part of the CGFZ and some of it continues to flow into the eastern Iceland Basin; the ISOW from north flows southwestward along the northern and western boundary of the Iceland Basin, and turns westward through gaps on the Reykjanes Ridge and the northern part of the CGFZ. In the lower layer ($\sigma_2 \geq 37.00$), the

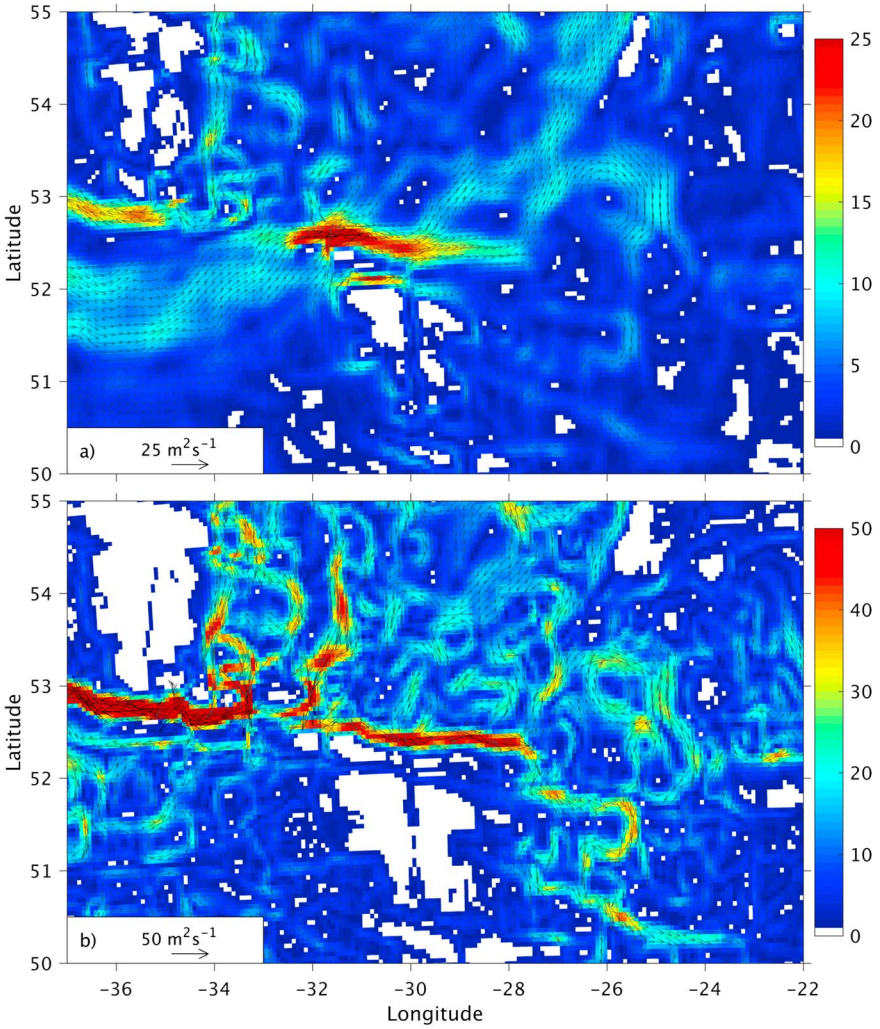

Figure 17. Modeled 35-year mean transport per unit width (in m^2/s) for two layers of ISOW in the CGFZ area: (a) $36.93 \leq \sigma_2 < 37.00$ kg/m^3 and (b) $\sigma_2 \geq 37.00$ kg/m^3.

relatively saline and dense ISOW from the Iceland Basin flows southward, with one branch flowing westward through the CGFZ and the other southward along the eastern flank of the MAR. Thus, the overall transport budget for ISOW density range ($\sigma_2 \geq 36.93$) in the southern Iceland Basin can be summarized as (a) two pathways entering the area (3-Sv saline ISOW from north and 1.5-Sv relatively fresh recirculating ISOW from west across the southern part of the CGFZ) and (b) three pathways out of the area (0.5 Sv to the west over the Reykjanes Ridge, 2.4 Sv to the west through the CGFZ, and 1.7 Sv to the south along the eastern flank of the MAR).

The time series of the modeled monthly and annual mean transports across the southern four sections are shown in Figures 15d–15g. Compared to the upstream transports (Figures 15a–15c), the variability of the modeled westward transport across the Reykjanes Ridge is relatively small and it exhibits a small long-term weakening trend of 0.12 Sv per decade (opposite to that through the CGFZ). The transport variability at 53.3°N is significantly higher than the upstream at 58°N and the two time series are not correlated, with a low correlation coefficient of 0.24 (0.27) for monthly (annual) mean transports. Most of the variability increase is on intraseasonal time scales: the standard deviation for monthly mean transports increases from 0.55 to 0.99 Sv, whereas the standard deviation for annual mean transports increases slightly from 0.23 to 0.25 Sv. The transport at 53.3°N also exhibits a small long-term increasing trend (0.06 per decade), offsetting about half of that through the Reykjanes Ridge.

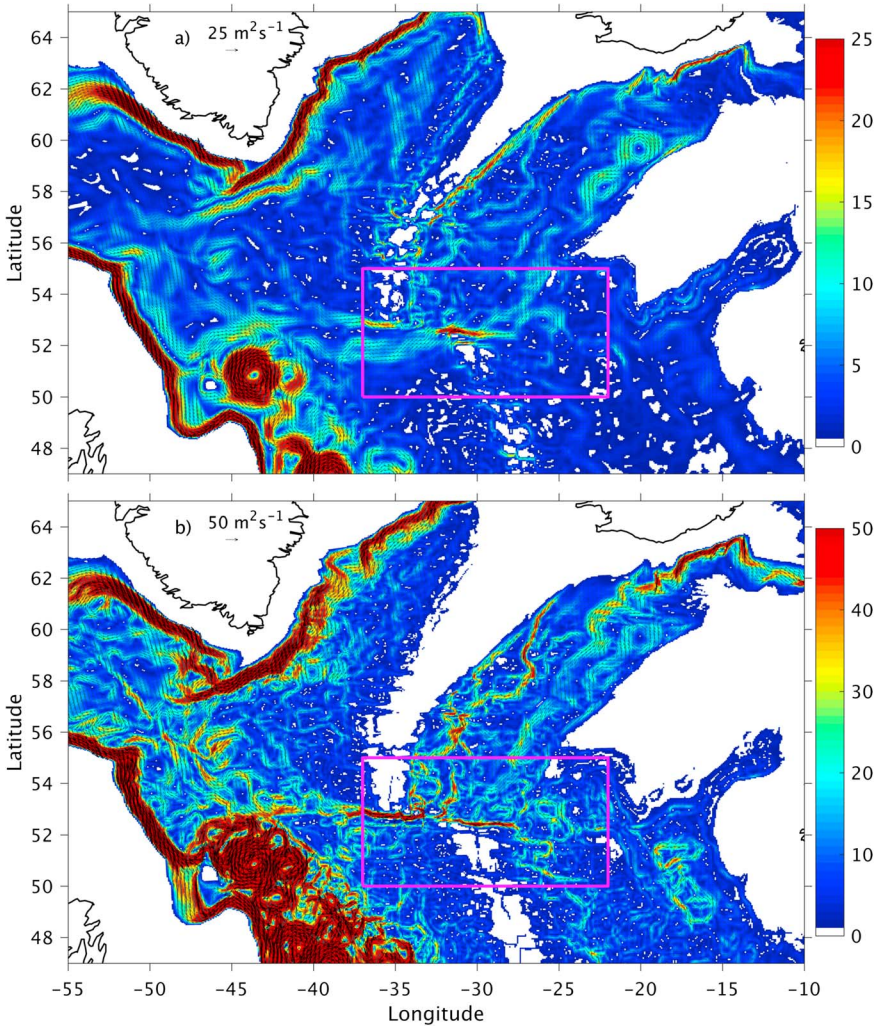

Figure 18. Modeled 35-year mean transport per unit width (in m^2/s) for two overflow layers in the subpolar North Atlantic: (a) $36.93 \leq \sigma_2 < 37.00$ kg/m^3 and (b) $\sigma_2 \geq 37.00$ kg/m^3 (the pink box marks the CGFZ region shown in Figure 17).

Further downstream at the CGFZ and 52°N sections, the transport variabilities are much higher than the upstream sections, on both intraseasonal and interannual time scales. The standard deviation values of the monthly and annual mean transports at CGFZ and 52°N sections (Figures 15f and 15g) are about a factor of 3 compared to the upstream values in the northern and central Iceland Basin (Figures 15a–15c). The combined variability at the CGFZ and 52°N sections is highly correlated with the variability at 53.3°N, with a correlation coefficient of 0.86 (0.81) for monthly (annual) means. The variability between the CGFZ and 52°N sections is anticorrelated, with a negative correlation coefficient of −0.65 (−0.86) for monthly (annual) means. These results suggest that the westward transport at CGFZ and the southward transport at 52°N are both part of the ISOW that flows southward across 53.3°N and the two pathways are covarying out of phase with each other. The transport variability at these three sections is not correlated with that of the upstream ISOW source. This is consistent with the fact that the variability in the south Iceland Basin is dominated by the meridional displacement of the NAC front as discussed in section 4.

6. Summary and Discussion

The Iceland-Scotland overflow water (ISOW) is one important component of the North Atlantic Deep Water, which flows southward as the lower limb of the Atlantic meridional overturning circulation (AMOC). Observations and numerical results suggest that the ISOW has multiple flow pathways out of the Iceland

Basin: the westward flow through the Charlie-Gibbs Fracture Zone (CGFZ), westward flows through gaps in the Reykjanes Ridge north of the CGFZ, and a southward flow along the eastern flank of the Mid-Atlantic Ridge south of the CGFZ. The measured transports through the CGFZ are dominated by high temporal variability. This study investigates where this transport variability comes from and how it is related to the variability at the upstream locations in the Iceland Basin and the variability of the other flow pathways.

The analyses are based on the interannually forced, 1/12° eddying simulation of the North Atlantic from 1978 to 2012 (Xu et al., 2013). It is shown in this study that the model results represent well the key feature of the observed ISOW in the Iceland Basin and through the CGFZ. In particular, the transport variability of the modeled ISOW through the CGFZ is in excellent agreement with the observations in both 1988–1989 and 2010–2012. The analyses show the following:

1. Variability of the ISOW transports through the CGFZ is closely correlated with the variability of the barotropic transports in the CGFZ associated with the meridional displacement of the NAC front, which can be inferred from sea surface height differences across the CGFZ. A potential source for the variability of the ISOW transport through the CGFZ is the fluctuations in the large-scale zonal wind stress in the western European Basin east of CGFZ.
2. ISOW transport through the CGFZ is highly variable on both intraseasonal and interannual time scales, with a standard deviation of 1.8 and 0.6 Sv for monthly and annual mean transports, respectively. These values are a factor of 3 higher compared to the values in the northern and central Iceland Basin, and their variabilities are not correlated, confirming that the ISOW variability in the CGFZ does not come from the upstream source.
3. The variability of the southward ISOW transport along the eastern flank of the Mid-Atlantic Ridge is comparable to that in the CGFZ, and the two time series are strongly anticorrelated, suggesting an out-of-phase covariation between these two flow pathways. This is consistent with Zou et al. (2017) who, based on numerical floats in FLAME model results, find that the fraction of the southward water export into the western European Basin is anticorrelated with the westward export through the CGFZ.

In terms of long-term mean transports, the southward flow of saline ISOW (~3 Sv) and an eastward flow of fresher water within the ISOW density range (~1.5 Sv) combined to provide the source for the three ISOW flow pathways in the southern Iceland Basin, about 0.5 Sv to the west over the Reykjanes Ridge, 2.4 Sv to the west through the CGFZ, and 1.7 Sv to the south along the eastern flank of the Mid-Atlantic Ridge (~1 Sv is the saline ISOW from the north). These time mean flow pathways and transport patterns are consistent with the results based on the climatological simulation in Xu et al. (2010), except that here less ISOW flows westward across the Reykjanes Ridge, and more flows through the CGFZ. The southward ISOW transport along the eastern flank of the MAR is consistent with the tracer observations of Fleischmann et al. (2001) as well as the velocity measurements recently reported in Zou et al. (2017). Compared to its westward counterpart through the CGFZ, this southward flow of the ISOW has received less attention, and further measurements are needed to determine its volume transport, its destination farther south, and its role in water properties of the deep eastern North Atlantic.

Acknowledgments
X.X. and E.P.C. are supported by the U.S. National Science Foundation Physical Oceanography Program (award 1537136) and the National Oceanic and Atmospheric Administration Climate Program Office MAPP Program (award NA15OAR4310088). A.B. and H.F. are supported by U.S. National Science Foundation through grant OCE-0926656 and by Woods Hole Oceanographic Institution through the Henry Bryant Bigelow Chair for Excellence in Oceanography award (to A.B.) in 2014. The numerical simulations were performed on supercomputers at the Navy DoD Supercomputing Resource Center, Stennis Space Center, Mississippi, using computer time provided by the U.S. DoD High Performance Computing Modernization Program. The CGFZ mooring data are available from NCEI (http://accession.nodc.noaa.gov/0164585). The altimeter products used here were produced by Ssalto/Duacs and distributed AVISO, with support from CNES (http://www.aviso.altimetry.fr/duacs). The model outputs are stored in the U.S. Navy DSRC archive server, and the model results presented in this study are available in HYCOM server (ftp://ftp.hycom.org/pub/xbxu/ATLg0.08/CGFZ).

References

Bacon, S., & Saunders, P. M. (2010). The deep western boundary current at cape farewell: Results from a moored current meter array. *Journal of Physical Oceanography*, *40*(4), 815–829. https://doi.org/10.1175/2009JPO4091.1

Beaird, N. L., Rhines, P. B., & Eriksen, C. C. (2013). Overflow waters at the Iceland-Faroe ridge observed in multi-year Seaglider surveys. *Journal of Physical Oceanography*, *43*(11), 2334–2351. https://doi.org/10.1175/JPO-D-13-029.1

Belkin, I. M., & Levitus, S. L. (1996). Temporal variability of the subarctic front near the Charlie-Gibbs fracture zone. *Journal of Geophysical Research*, *101*(C12), 28,317–28,324. https://doi.org/10.1029/96JC02794

Biastoch, A., Boning, C. W., Getzlaff, J., Molines, J.-M., & Madec, G. (2008). Causes of interannual–decadal variability in the meridional overturning circulation of the midlatitude North Atlantic Ocean. *Journal of Climate*, *21*(24), 6599–6615. https://doi.org/10.1175/2008JCLI2404.1

Bleck, R. (2002). An oceanic general circulation model framed in hybrid isopycnic-Cartesian coordinates. *Ocean Modelling*, *37*, 55–88.

Bower, A. S., & Furey, H. (2017). Iceland-Scotland overflow water transport variability through the Charlie-Gibbs fracture zone and the impact of the North Atlantic current. *Journal of Geophysical Research: Oceans*, *122*, 6989–7012. https://doi.org/10.1002/2017JC012698

Bower, A. S., & von Appen, W.-J. (2008). Interannual variability in the pathways of the North Atlantic current over the mid-Atlantic ridge and the impact of topography. *Journal of Physical Oceanography*, *38*(1), 104–120. https://doi.org/10.1175/2007JPO3686.1

Chassignet, E. P., Smith, L. T., Halliwell, G. R., & Bleck, R. (2003). North Atlantic simulation with the HYbrid Coordinate Ocean model (HYCOM): Impact of the vertical coordinate choice, reference density, and thermobaricity. *Journal of Physical Oceanography*, *33*(12), 2504–2526. https://doi.org/10.1175/1520-0485(2003)033<2504:NASWTH>2.0.CO;2

Chassignet, E. P., & Xu, X. (2017). Impact of horizontal resolution (1/12° to 1/50°) on gulf stream separation, penetration, and variability. *Journal of Physical Oceanography*, *47*(8), 1999–2021. https://doi.org/10.1175/JPOD-17-0031.1

Daniault, N., Mercier, H., Lherminier, P., Sarafanov, A., Falina, A., Zunino, P., et al. (2016). The northern North Atlantic Ocean mean circulation in the early 21st century. *Progress in Oceanography*, *146*, 142–158. https://doi.org/10.1016/i.pocean.2016.06.007

Dickson, R. R., & Brown, J. (1994). The production of North Atlantic deep water: Source, rates, and pathways. *Journal of Geophysical Research*, *99*(C6), 12,319–12,341. https://doi.org/10.1029/94JC00530

Dickson, R. R., Dye, S., Jónsson, S., Köhl, A., Macrander, A., et al. (2008). The overflow flux west of Iceland: Variability, origins and forcing. In R. R. Dickson, J. Meincke, & P. Rhines (Eds.), *Arctic-Subarctic Ocean Fluxes: Defining the Role of the Northern Seas in Climate* (pp. 443–474). New York: Springer. https://doi.org/10.1007/978-1-4020-6774-7_20

Fleischmann, U., Hildebrandt, H., Putzka, A., & Bayer, R. (2001). Transport of newly ventilated deep water from the Iceland Basin to the west European Basin. *Deep Sea Research Part I: Oceanographic Research Papers*, *48*, 1793–1819.

Häkkinen, S., & Rhines, P. B. (2004). Decline of subpolar North Atlantic gyre circulation during the 1990s. *Science*, *304*(5670), 555–559. https://doi.org/10.1126/science.1094917

Halliwell, G. R. (2004). Evaluation of vertical coordinate and vertical mixing algorithms in the hybrid Coordinate Ocean model (HYCOM). *Ocean Modelling*, *7*(3-4), 285–322. https://doi.org/10.1016/j.ocemod.2003.10.002

Hansen, B., & Østerhus, S. (2000). North Atlantic-Nordic seas exchanges. *Progress in Oceanography*, *45*(2), 109–208. https://doi.org/10.1016/S0079-6611(99)00052-X

Hansen, B., & Østerhus, S. (2007). Faroe Bank Channel overflow 1995–2005. *Progress in Oceanography*, *75*(4), 817–856. https://doi.org/10.1016/j.pocean.2007.09.004

Johns, W., Houk, A., Koman, G., Zou, S., & Lozier, S. (2017). Transport of Iceland-Scotland Overflow waters in the Deep Western Boundary Current along the Reykjanes Ridge, 19th EGU General Assembly, proceedings from the conference held 23–28 April, 2017 in Vienna, Austria (9415 pp.).

Kanzow, T., & Zenk, W. (2014). Structure and transport of the Iceland Scotland Overflow plume along the Reykjanes Ridge in the Iceland Basin. *Deep Sea Research*, *86*, 82–93. https://doi.org/10.1016/j.dsr.2013.11.003

Livingston, H. D., Swift, J. H., & Ostlund, H. G. (1985). Artificial radiouclide tracer supply to the Denmark Strait overflow between 1972 and 1981. *Journal of Geophysical Research*, *90*(C4), 6971–6982. https://doi.org/10.1029/JC090iC04p06971

Rhein, M., Kieke, D., Kabus, S. H., Roessler, A., Mertens, C., Meissner, R., et al. (2011). Deep water formation, the subpolar gyre, and the meridional overturning circulation in the subpolar North Atlantic. *Deep Sea Research, Part II*, *58*(17-18), 1819–1832. https://doi.org/10.1016/j.dsr2.2010.10.061

Roessler, A., Rhein, M., Kieke, D., & Mertens, C. (2015). Long-term observations of North Atlantic current transport at the gateway between western and eastern Atlantic. *Journal of Geophysical Research: Oceans*, *120*, 4003–4027. https://doi.org/10.1002/2014JC010662

Rosmond, T., Teixeira, J., Peng, M., Hogan, T., & Pauley, R. (2002). Navy operational global atmospheric prediction system (NOGAPS): Forcing for ocean models. *Oceanography*, *15*(1), 99–108. https://doi.org/10.5670/oceanog.2002.40

Saunders, P. M. (1994). The flux of overflow water through the Charlie-Gibbs fracture zone. *Journal of Geophysical Research*, *99*(C6), 12,343–12,355. https://doi.org/10.1029/94JC00527

Saunders, P. M. (1996). The flux of dense cold water overflow southeast of Iceland. *Journal of Physical Oceanography*, *26*(1), 85–95. https://doi.org/10.1175/1520-0485(1996)026<0085:TFODCO>2.0.CO;2

Saunders, P. M. (2001). The dense northern overflows. In G. Siedler, J. Church, & J. Gould (Eds.), *Ocean Circulation and Climate* (pp. 401–417). New York: Academic.

Schott, F., Stramma, L., & Fischer, J. (1999). Interaction of the North Atlantic current with deep Charlie Gibbs fracture zone throughflow. *Geophysical Research Letters*, *26*(3), 369–372. https://doi.org/10.1029/1998GL900223

Sherwin, T. J., & Turrell, W. R. (2005). Mixing and advection of a cold water cascade over the Wyville Thomson ridge. *Deep Sea Research*, *52*(8), 1392–1413. https://doi.org/10.1016/j.dsr.2005.03.002

Treguier, A. M., Theetten, S., Chassignet, E. P., Penduff, T., Smith, R., Talley, L., et al. (2005). The North Atlantic subpolar gyre in four high-resolution models. *Journal of Physical Oceanography*, *35*(5), 757–774. https://doi.org/10.1175/JPO2720.1

Uppala, S. M., KÅllberg, P. W., Simmons, A. J., Andrae, U., Bechtold, V. D. C., Fiorino, M., et al. (2005). The ERA-40 re-analysis. *Quarterly Journal of the Royal Meteorological Society*, *131*(612), 2961–3012. https://doi.org/10.1256/qj.04.176

Wu, Z., & Huang, N. E. (2009). Ensemble empirical mode decomposition: A noise-assisted data analysis method. *Advances in Adaptive Data Analysis*, *01*(01), 1–41. https://doi.org/10.1142/S1793536909000047

Xu, X., Hurlburt, H. E., Schmitz, W. J. Jr., Zantopp, R. J., Fischer, J., & Hogan, P. J. (2013). On the currents and transports connected with the Atlantic meridional overturning circulation in the subpolar North Atlantic. *Journal of Geophysical Research: Oceans*, *118*, 502–516. https://doi.org/10.1002/jgrc.20065

Xu, X., Schmitz, W. J. Jr., Hurlburt, H. E., Hogan, P. J., & Chassignet, E. P. (2010). Transport of Nordic seas overflow water into and within the Irminger Sea: An eddy-resolving simulation and observations. *Journal of Geophysical Research*, *115*, C12048. https://doi.org/10.1029/2010JC006351

Zou, S., Lozier, S., Zenk, W., Bower, A., & Johns, W. (2017). Observed and modeled pathways of the Iceland Scotland overflow water in the eastern North Atlantic. *Progress in Oceanography*, *159*, 211–222. https://doi.org/10.1016/j.pocean.2017.10.003